Classifying M1 Muscarinic Receptor Antagonism using Generative Embeddings from DCM in an EEG-MMN Paradigm

Benjamin Kressig
ETH Zürich

Jeremias Baur
ETH Zürich

Jamie Balfour
ETH Zürich

Abstract

Heterogeneity in treatment response is a major challenge in schizophrenia. Developing methods for individualized treatment prediction is therefore a key goal. One hypothesis suggests that this variability may arise from differential impairments in cholinergic vs. dopaminergic neuromodulation of NMDA receptor function [Weber et al. 2022] [Stephan et al. 2009]. However, there are very limited options to non-invasively assay receptor function in the brain. In this project, we propose a non-invasive method using Dynamic causal modeling (DCM) to infer subject-specific neuronal parameters from electroencephalogram (EEG) data in a mismatch negativity (MMN) paradigm. These posterior parameters of the DCM then served as features for machine learning classifiers to differentiate participants given biperiden, a muscarinic M1 receptor antagonist, from those given a placebo. Our primary analysis achieved an estimated classification accuracy of 65.22% on out-of-sample predictions. These findings demonstrate the potential of using generative embeddings from DCM of MMN data to probe muscarinic receptor function, which could ultimately aid in identifying patient subgroups that respond differently to cholinergic treatments.

1 Introduction

Contemporary psychiatric treatment allocations, based on symptoms, lack a focus on underlying physiological mechanisms. This contributes to a trial-and-error approach in prescribing medications, despite most drugs targeting specific neuromodulatory transmitters. Understanding patient heterogeneity and identifying specific neurobiological deficits is crucial for developing personalized treatments [Weber et al. 2022]. Schizophrenia is a prime example of a disorder linked to complex dysfunctions in neurotransmitter systems, including dopamine, glutamate, and acetylcholine. However, non-invasive in vivo methods to assay the functional status of specific receptors are currently only very limited [Schöbi et al. 2021]

The auditory MMN is an event-related potentials (ERP), which is the brain's response to an odd tone in a sequence of tones. The MMN is reduced in schizophrenia and is sensitive to alterations in key systems like the NMDA receptor function. Thus it has been proposed as a promising biomarker [Näätänen et al. 2015]. Furthermore, recent work suggests the MMN is also sensitive to muscarinic cholinergic system alterations [Weber et al. 2022].

Dynamic Causal Modeling (DCM) offers a powerful generative framework to infer latent neuronal parameters, including those related to synaptic function, from neurophysiological data like EEG [Garrido et al. 2009]. By subsequently applying machine learning techniques to these DCM-derived posterior parameter estimates, an approach termed generative embedding, it may be possible to classify individuals based on subtle, model-inferred differences in their underlying neurophysiology [Heinzle and Stephan 2018].

This project aims to leverage the generative embedding strategy. Specifically, we use MMN-EEG data from [Weber et al. 2022] and investigate whether DCM posterior parameters can be used to train a classifier, capable of differentiating participants given the muscarinic M1 receptor antagonist biperiden from those given a placebo.

The original dataset also contains a third group of patients taking amisulpride, a D2/D3 dopamine receptor antagonist. However, [Weber et al. 2022] only found a significant change in the MMN for biperiden compared to placebo and not for amisulpride. For this reason we focus our study only on the placebo and biperiden subjects in the dataset.

Author contributions using the CRediT framework:
B. Kressig: Conceptualization, Methodology, Software, Validation, Visualization, Formal Analysis, Investigation, Writing
J. Baur: Conceptualization, Methodology, Software, Validation, Visualization, Formal Analysis, Investigation, Writing
J. Balfour: Conceptualization, Methodology, Software, Validation, Visualization, Formal Analysis, Investigation, Writing

227-0973-00L Translational Neuromodeling, 1st of June, 2025, Zurich, Switzerland
2026.

2 Previous Work

2.1 Modeling The Mismatch Negativity

Using DCM to model ERP is not a novel concept [David et al. 2005]. [Garrido et al. 2008] did extensive research on modeling the auditory MMN in EEG data. They used electrophysiological and imaging data to create a generative model that can be used to explain the MMN.

Already in 2016, [Gilbert et al. 2016] identified ion channel neuropathies in humans by comparing posterior parameter estimates of DCM models trained on MEG data during MMN paradigms. However, they had a small dataset with only 2 sick subjects. Similarly, [Schöbi et al. 2021] trained DCMs on EEG data from mice under different muscarinic receptor modulating drug conditions during an MMN paradigm. They showed that it was possible to identify which drug was given to these mice, using a linear Support Vector Machine (SVM) trained on the generative model parameters.

2.2 Biperiden's Impact on our Model

Biperiden is a muscarinic acetylcholine receptor antagonist. It binds to these receptors and prevents their activation. There are five receptor subtypes M1-M5. Of these, M1, M2, and M4 are the most prevalent in the human cortex [Volpicelli and Levey 2004], where the DCM sources described by [Garrido et al. 2009] are located.

Out of the receptor subtypes in the cortex, [Bolden et al. 1992] found that biperiden binds strongest to M1 receptors, having an affinity to M1 five times stronger than M4 and 12 times stronger than that to M2 . Additionally, M1 counts for approximately 35-60% of all muscarinic receptors in the cortex, while M2 and M4 account for roughly 20% each. Additionally, immunolabeling shows M1 and M2 are localized to different cell subtypes, specifically M1 being present in pyramidal terminals on all cortical levels, and M2 are localized to inhibitiory interneurons in layers IV and V/VI [Lebois et al. 2018; Volpicelli and Levey 2004].

The strong affinity of biperiden to M1 receptors and their relative abundance in the brain over other muscarinic subtypes lead us to further concentrate on the impact that blocking M1 receptors would have. M1 receptors are $G_{q/11}$ protein-coupled postsynaptic receptors, which upon activation by binding with acetylcholine releases the G protein and activates several pathways that lead to membrane depolarization and increase cell excitability. They do so by activating phospholipase C, which goes on to increase intracellular Ca^{2+} and closes different types of K^+ channels. This causes depolarization and leads to ejection of Mg^{2+} from NMDA receptors and subsequently an increase in NMDA currents [Galvin et al. 2020; Thiele 2013].

This previous work creates the expectation that most of the variability in our models will appear on a neuronal level, leading us to adopt a conductance-based neuronal model for this project. This would better capture these dynamics compared to a convolution-based model, specifically in the conductivity parameters for each channel type and the gain parameters for each population[Pereira et al. 2021]. However, this conductivity model has a fixed leak current, which is where the ionic K^+ current is modeled. This means that we will likely see our model attempt to fit this by smaller changes in many different parameters.

Another important note is that biperiden is an antagonist, that blocks the activation of M1 receptors, and its use would result in membrane hyperpolarization and a net inhibitory effect. We would also expect these effects to be stronger in our pyramidal cell populations. However, they could also be observed as a potentiation of our inhibitory neurons.

3 Methods

3.1 Dataset Description

The used dataset is from "Study 1: amisulpride and biperiden" by [Weber et al. 2022]. A detailed description of this study is given in their publication. In the following, we give a summary of what is important for our experiments. The original study involved 81 healthy male volunteers (mean age 22.7 years, SD = 3.6, range = 18-38 years). Participants were randomly assigned in a double-blind, between-subject design to receive either placebo, biperiden, or amisulpride (not analyzed in our work). Of the initial 81 participants, 10 were excluded due to either: a change in the stimulus sequence after the first few participants (N=6), technical issues during measurement (N=2), and insufficient correction of eye blink artifacts (N=2). Thus, our analysis focused on the remaining participants in the placebo (N=25) and biperiden (N=21) groups.

3.1.1 Experimental Paradigm. Participants underwent an auditory oddball paradigm while engaged in a visual distraction task. They passively listened to a sequence of 1800 sinusoidal tones (70 ms duration, 500 ms inter-stimulus interval), consisting of high (528 Hz) and low (440 Hz) tones presented with varying probabilities to elicit standard and deviant responses. A tone was defined as deviant only if it followed at least five repetitions of the other tone (N_{deviant} = 119). Similarly, a tone was considered as standard if it was the 6th repetition of the same tone (N_{standard} = 106). This definition follows previous studies [Garrido et al. 2008].

3.1.2 EEG Acquisition. The EEG recordings used an EASYCAP system with 64 scalp electrodes plus one electrooculography (EOG) channel (10-20 layout), sampled at 500 Hz with a nose reference.

3.2 Data Preprocessing

The raw EEG data is pre-processed according to the pipeline detailed in [Weber et al. 2022], using SPM12 and MATLAB. Key steps included:

(1) Re-referencing to the average of all scalp electrodes.
(2) High-pass filtering (Butterworth filter, 0.1 Hz cutoff)
(3) Downsampling to 250 Hz.
(4) Low-pass filtering (Butterworth filter, 30 Hz cutoff).

Next, the continuous data were epoched from -100ms to 400ms around tone onsets (0ms). No baseline correction was applied to these epochs. Eye-movement artefacts and eyeblinks were corrected using signal space projection (SSP). Epochs with signals exceeding ±75 μV at any channel were rejected.

To obtain the event-related potentials (ERPs) that serve as input for the DCM analysis. The cleaned and artifact-rejected epochs of each channel of each subject were averaged separately for relevant conditions (e.g., standard and deviant tones). This averaging process yields the characteristic ERP waveforms for each condition per participant.

3.3 Dynamic Causal Modeling

DCM is a generative modeling technique that can infer the effective connectivity of brain regions and (latent) neuronal states using a Bayesian framework [Heinzle and Stephan 2018]. The model describes neuronal dynamics as a system of interconnected differential equations. A forward model is used to map the activity at the source level to the measured potential at the scalp surface. The parameters describing those dynamics can then be inferred from EEG data using a variational Bayes scheme. There are many variants and possibilities for DCM modeling. Therefore, it is important to have a clear hypothesis on what one wants to test and model.

According to [Garrido et al. 2009], the event-related potentials during an auditory MMN paradigm can be explained within a predictive coding framework. Based on this theory, they investigated a DCM model space with combinations that included the brain regions of each left and right primary auditory cortex (A1), superior temporal gyrus (STG) and only the right inferior frontal gyrus (IFG). With Bayesian model comparison they came to the conclusion, that the FBi model shown in Figure 1 has the highest evidence. Therefore, we rely on this previous research and use the found brain region connectivity model without any further exploration of

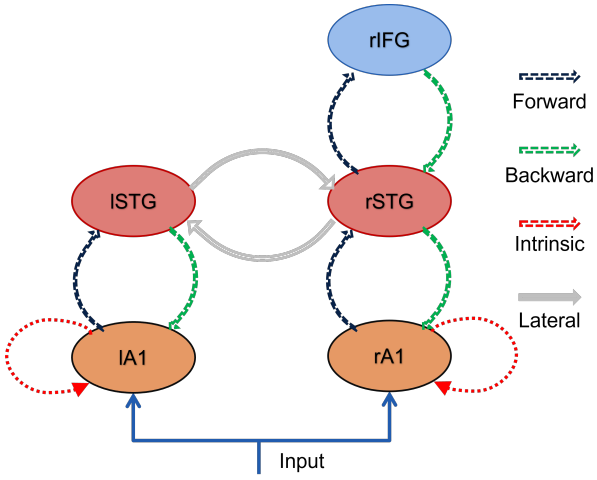

Figure 1: Inter-source connectivity for the 5 source hierarchical FBi model implemented in [Garrido et al. 2008]. Additionally in gray, we show the lateral connectivity that was present in our initial model (lateral FBi). Dashed lines represent connections that are modulated by the deviant condition.

model structures. (Note: Initially, there was a setup mistake in our DCM Matlab code, a prior bilateral connection was defined between STG (Grey connections in Figure 2). The results of the lateral FBi model were put in the Appendix A as a reference for future studies. The subsequent sections, analysis, and discussion cover the correct FBi model.)

For this study, we are interested in the underlying workings of the neuronal synapses under the pharmacological intervention of biperiden. Hence, we are using a neuronal mass conductance-based canonical microcircuit model that includes the NMDA receptor (CMM_NMDA in SPM12). This model has an explicit representations of the ionotropic receptors NMDA, AMPA and GABA. Each cortical column (source) consists of a superficial pyramidal cell (SPC), a spiny stellate cell (SC), an inhibitory-interneuron (IC), and a deep pyramidal cell (DPC) [Pereira et al. 2021] as shown in Figure 2. This model gives us the ability to create a lower-dimensional generative embedding from the high-dimensional EEG measurements. All inferred parameters are described in Section 3.3.1. We have chosen a peak onset of 80ms based on the first observed deflection of the ERP in [Weber et al. 2022]. The first five principal eigenmodes of the projected channel data were chosen because we have five sources in our model. The SPM12 Matlab implementation was used [Wellcome Centre for Human Neuroimaging 2025]. The model is defined in `spm_fx_cmm_NMDA.m`. The priors were kept to the standard values defined in `spm_cmm_NMDA_priors.m`. As there was no

participant electrode placement data available, a standard equivalent current dipoles (ECD) forward model was chosen with the default "3-Shell Sphere" SPM preset. The location priors in MNI coordinates of the sources are given in table 1.

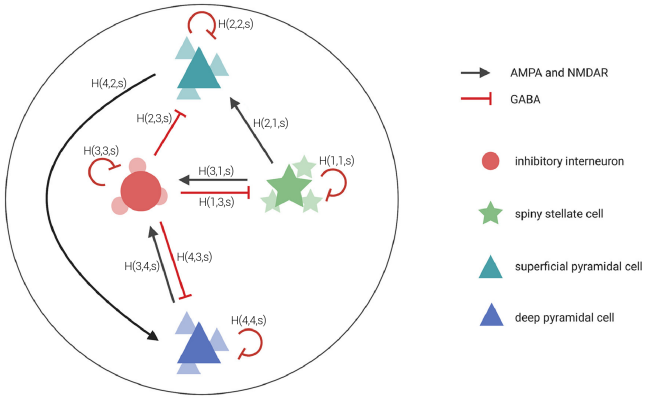

Figure 2: Intra-source connectivity for the 4-population CMM_NMDA model implemented in `spm_fx_cmm_nmda.m`. The shown synaptic density parameters $H(p_i, p_j, s)$ are inferred per brain region s via DCM inversion. Figure adapted from [Pereira et al. 2021].

Table 1: Prior coordinates for the locations of the equivalent current dipoles in MNI space (mm) as defined in [Garrido et al. 2008].

Left primary auditory cortex (lA1)	−42, −22, 7
Right primary auditory cortex (rA1)	46, −14, 8
Left superior temporal gyrus (lSTG)	−61, −32, 8
Right superior temporal gyrus (rSTG)	59, −25, 8
Right inferior frontal gyrus (rIFG)	46, 20, 8

3.3.1 Overview of Parameters.

The parameters that were inferrable in our defined model are explained in this section. First, they are inferred via the inversion of the previously described FBi model for every participant. Afterwards, all non-constant (over participant) posterior estimates, the generative embeddings, are used as features for the machine learning models described in Section 3.4. In total, 108 parameters are used as features. The sources (brain regions) have the following number mappings s: lA1: 1, rA1: 2, lSTG: 3, rSTG: 4 and rIFG: 5.

- The matrix element $A\{1,2\}(s_1, s_2)$ represents the extrinsic {forward, backward} connection from source s_1 to s_2, respectively.
- The matrix element $AN\{1,2\}(s_1, s_2)$ represents the extrinsic {forward, backward} connection from source s_1 to s_2 of the NMDA receptor, respectively.
- The matrix element $B\{1\}(s_1, s_2)$ represents the trial-dependent modulatory effect on the present connections from source s_1 to s_2.
- The matrix element $BN\{1\}(s_1, s_2)$ represents the trial-dependent modulatory effect on the present connections from source s_1 to s_2 of the NMDA receptor.
- $H(p_i, p_j, s)$ describes the intrinsic synaptic densities between each neuronal population p_i, p_j in each brain region s as visualized in Figure 2. It correspond to the connective strength between cell types. The neuronal populations have the mapping: SC: 1, SPC: 2, IC: 3, DPC: 4.
- The matrix $T(s, c_i)$ represents the negative log-transformed synaptic time constant in source s and channel c_i with the c_i mapping: excitatory AMPA rate constant: 1, inhibitory GABA rate constants: 2 and excitatory rate NMDA constants: 3.
- $CV \in \mathbb{R}^4$ stores the membrane capacitance of each population type p_i.
- $S(1)$ is the population variance.
- $C(1)$ and $C(2)$ is the stimulus input connection of lA1 and rA1, respectively.
- $R(1)$ and $R(2)$ are the exogenous onset and dispersion parameters, respectively.
- $E(1)$ is the exogenous background activity.
- $D(1)$ and $D(2)$ are intrinsic and extrinsic delays, respectively.

3.4 Machine Learning Classification

We implemented a machine learning pipeline, with a focus on explainable models, to classify participants (biperiden vs. placebo) based on posterior parameters from their inverted FBi DCMs. Given the limited size of the dataset, we chose a nested cross-validation (CV) approach to optimize the hyperparameters of the classifiers while obtaining an unbiased estimate of the generalization performance. The workflow is as follows:

(1) **Feature Extraction**: Posterior estimated parameters from fitted DCMs served as input features. We removed features that are constant across the participants since they don't contain any information relevant for the classifier.
(2) **Nested Cross-Validation**: This provided unbiased performance estimates and implements hyperparameter optimization for a SVM and a Random Forest (RF) classifier.
(3) **Model Interpretation**: Final models, trained on all data using the optimized hyperparameters derived from the nested CV, were used for feature importance analysis.

3.4.1 Algorithms.

Support Vector Machine (SVM). A SVM with linear kernel was used, which aims to find an optimal separating hyperplane between classes. The `BoxConstraint` hyperparameter, which controls the trade-off between margin maximization and misclassification penalty, was tuned during the nested CV procedure. (More details on this optimization below in paragraph Inner Loop.) This form of a SVM with a linear kernel only gives linear decision boundaries. However it has the benefit, that assessing their feature importance is straightforward, as described in more detail below. Therefore we decided not to use kernelized SVMs, as their interpretation is much more involved. The MATLAB `fitcsvm` function was used for implementation.

Random Forest (RF). A RF classifier, an ensemble of multiple decision trees, was also employed to capture potential non-linear relationships, which our linear SVM cannot. RFs benefit from mechanisms like bagging and random feature selection at each tree split to improve generalization, although careful hyperparameter tuning is important. Implemented with MATLAB's `fitcensemble` (for optimization) and `TreeBagger` (for final model training), the hyperparameters tuned via nested CV are:

- `NumTrees`: The number of individual decision trees. A larger number generally improves performance and stability, up to a point, at the cost of increased computation.
- `MinLeafSize`: Minimum number of leaf node observations. This parameter controls tree complexity; smaller values allow for more complex trees that can potentially capture finer details but may also overfit, while larger values lead to simpler, more generalized trees.
- `NumPredictorsToSample`: The number of features (predictors) randomly selected for consideration at each split point when growing an individual tree. This introduces diversity among the trees in the forest.

3.4.2 Nested Cross-Validation.

Nested CV was implemented for unbiased performance estimation and hyperparameter optimization, which is particularly important for small datasets. It consists of an outer and an inner validation loop.

Outer Loop. The outer loop employed Leave-One-Out CV (LOOCV). In each of the N iterations (where N is the total number of samples), one sample was held out as the test set, and the remaining $N - 1$ samples formed the training set. This loop provides the primary, unbiased estimate of model performance, with aggregated predictions across all folds used to compute overall metrics.

Inner Loop. Within each outer LOOCV fold, an inner CV loop was performed exclusively on the current outer training set ($N - 1$ samples). This inner loop selected the optimal hyperparameters for the classifier in that specific outer fold using k-fold CV ($k = 4$ for RF and $k = 5$ for SVM). The optimization process itself utilized Bayesian optimization with the 'expected-improvement-plus' acquisition function to efficiently search the hyperparameter space. The hyperparameter set yielding the best average performance across these inner folds was chosen for that particular outer fold.

Hyperparameter Aggregation and Final Model Training. Since optimal hyperparameters can vary across outer folds, potentially with some larger outliers, the median of these selected values was determined to define a single set of hyperparameters for the final model. For the SVM, the median `BoxConstraint` selected across outer folds was 0.0100. For the RF, the median selected values were `NumTrees` (217), `MinLeafSize` (13), and `NumPredictorsToSample` (58). Afterwards, these aggregated median hyperparameters were used to train a final model on the entire dataset. Importantly, this final model was only used for feature importance analysis, while the main performance metrics reported in Section 4 are derived from the outer-loop predictions of the nested CV, ensuring an unbiased assessment.

3.4.3 Explainability of Classifiers.

To gain insights into which DCM-derived generative embedding features were the most discriminative, feature importance was estimated for both classifiers using the final models trained with aggregated hyperparameters.

SVM Feature Importance. For the linear SVM, feature importance was directly inferred from the absolute magnitudes of the weights (β) assigned to each feature in the learned hyperplane. These were obtained from the `Beta` property of the trained `fitcsvm` model object.

Random Forest Feature Importance. For the RF, feature importance was assessed using the Out-of-Bag (OOB) Permuted Predictor Delta Error (permutation importance). This method measures the increase in OOB prediction error when a feature's values are randomly permuted in the OOB samples. This was obtained from the `OOBPermutedPredictorDeltaError` property of the trained `TreeBagger` model object.

3.5 Statistical Tests

The following two statistical tests were applied:

3.5.1 Permutation Test.

A permutation test was implemented to test the significance of the prediction accuracy

of the SVM and RF each. This is a robust measure to test the significance of the prediction accuracy in small sample scenarios [Varoquaux et al. 2017]. First, the accuracy score of the nested CV was saved as A_{obs}. Second, $n = 1000$ iterations of the following procedure were performed:

(1) Randomly permute the Y labels (biperiden or placebo group).
(2) Train the classifier in LOOCV fashion.
(3) Save permuted prediction accuracy in array A_{perm}.

Next, the p-value $p = \frac{\sum_{i=1}^{n} \mathbb{1}[A_{\text{perm,i}} \geq A_{\text{obs}}]}{n}$ was calculated and compared to the significance level $\alpha = 0.05$. If $p \leq \alpha$, the classifier performance is statistically significant, otherwise the observed performance could be attributed to random chance.

3.5.2 Group-level difference. In addition to the investigation of the ML feature importance, a group-level parameter analysis was run. Every inverted DCM was organized into their respective placebo or biperiden group. Then a Bonferroni-corrected two-sided t-test was conducted for each of the 108 parameters between the two groups with a significance level of $\alpha = 0.05$.

4 Results

4.1 Nested Cross-Validation Performance

The generalization performance of the classifiers was evaluated using the predictions from the outer loop of the nested cross-validation. For interpreting the metrics (sensitivity, specificity, etc.), biperiden is treated as the positive class and placebo as the negative class.

4.1.1 Random Forest Classifier. The RF classifier achieved an accuracy of 58.70% ($p = 0.162$, chance level: 50%). Hence, the accuracy performance is not significantly different from random chance. The sensitivity (recall for the biperiden group) was 47.62%, and the specificity (recall for the placebo group) was 68.00%. The precision for the biperiden group was 55.56%, and the F1 score was 51.28%. The confusion matrix for the RF classifier is shown in Figure 3. The reported p-value is based on the permutation test shown in Figure 4.

4.1.2 Support Vector Machine Classifier. The SVM classifier achieved an accuracy of 65.22% ($p = 0.048$, chance level: 50%). The sensitivity (recall for the biperiden group) was 47.62%, and the specificity (recall for the placebo group) was 80.00%. The precision for the biperiden group was 66.67%, and the F1 score was 55.56%. The confusion matrix for the SVM classifier is shown in Figure 5. The reported p-value is based on the permutation test shown in Figure 6.

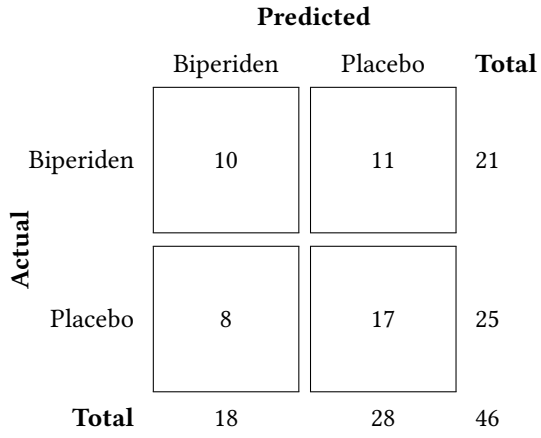

Figure 3: Confusion matrix for the RF classifier based on nested cross-validation.

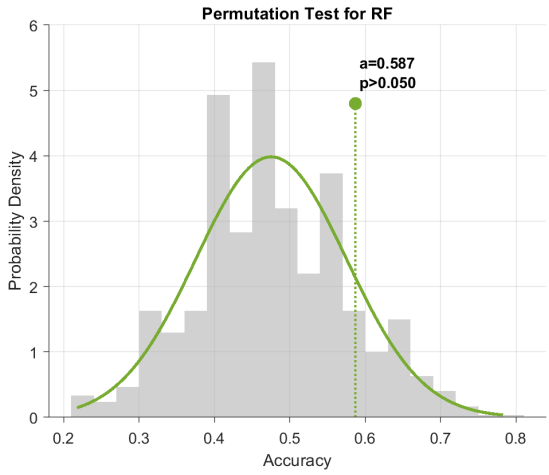

Figure 4: The gray histogram represents the accuracies of the RF classifier trained with permuted labels and LOOCV. These accuracies were fitted with a Gaussian distribution, overlaid here. Letter **a** refers to the RF nested CV accuracy with true labels and the p-value resulting from the permutation test.

4.2 Model Interpretation: Feature Importance

To identify the DCM-derived parameters most influential in distinguishing between the biperiden and placebo groups, feature importance was assessed using the final RF and SVM models. These models were trained on the entire dataset with the median hyperparameters derived from nested cross-validation. Figure 7 displays the top 20 features for the Random Forest (RF) model, and Figure 8 shows the top 20 features for the linear Support Vector Machine model.

		Predicted		
		Biperiden	Placebo	**Total**
Actual	Biperiden	10	11	21
	Placebo	5	20	25
	Total	15	31	46

Figure 5: Confusion matrix for the SVM classifier based on nested cross-validation.

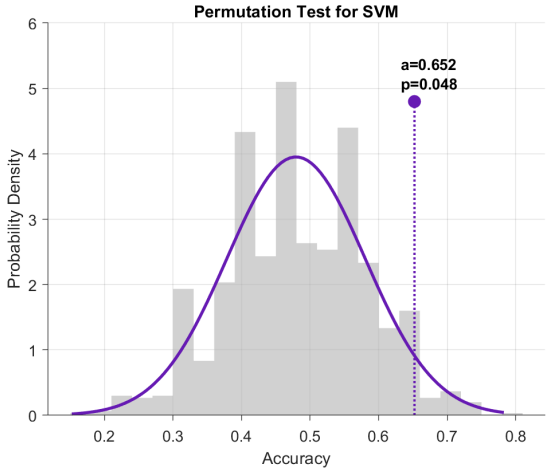

Figure 6: The gray histogram represents the accuracies of the SVM classifier trained with permuted labels and LOOCV. These accuracies were fitted with a Gaussian distribution, overlaid here. Letter **a** refers to the SVM nested CV accuracy with true labels and the p-value resulting from the permutation test.

4.3 Statistical Tests

The results of the permutation tests are reported as the p-values of the classifier accuracies in Section 4.1. The group-level parameter analysis with the two-sided t-test resulted in the parameter $H(1, 3, 4)$ being significantly different in the two groups (p<0.05, Bonferroni corrected). Every other parameter didn't differ significantly if Bonferroni corrected. The Table 2 in the Appendix lists all the results, including raw p-value, t-statistic, placebo mean and biperiden mean of the independent t-tests.

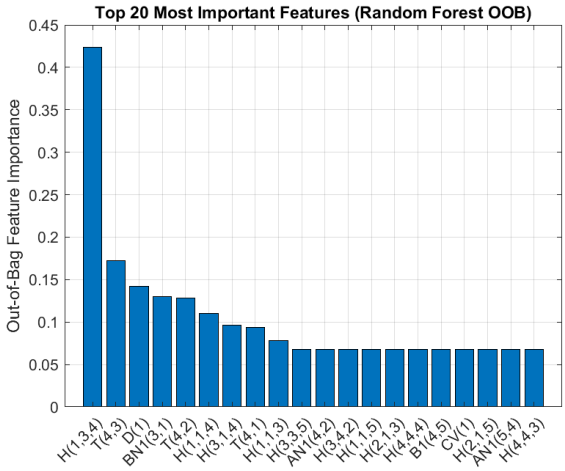

Figure 7: Top 20 features for the RF, assessed using Out of Bag (OOB) permutation importance. Please refer to Section 3.3.1 for an explanation of the features.

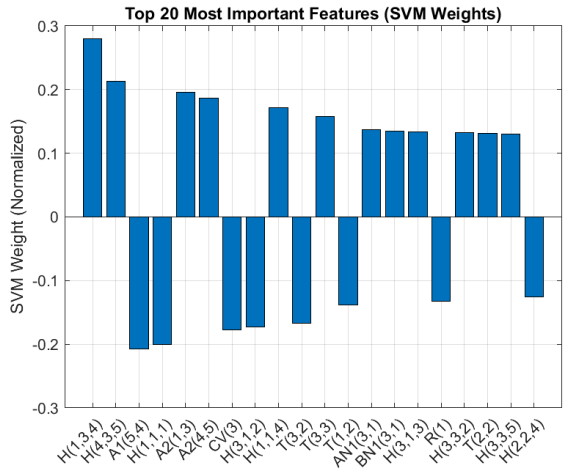

Figure 8: Top 20 features for the SVM, assessed by normalized weight corresponding to each feature. Please refer to Section 3.3.1 for an explanation of the features. A bigger positive (negative) weight means that the respective posterior estimates of the biperiden subjects are more positive (negative) than the placebo subjects, respectively.

4.4 Lateral FBi Model

It is noteworthy that the lateral FBi DCM model, explored due to an initial setup error from our side, yielded better performance characteristics, with the SVM achieving a nested cross-validated accuracy of 73.91%. (Detailed results provided in Appendix A) For our primary analysis, however, we decided to stick to the intended FBi model structure, as

it is motivated by prior research. Nevertheless, this alternative finding offers interesting perspectives for potential model refinement, which we further discuss in Section 6. We now proceed with the remaining discussion for our primary, theoretically-grounded model.

5 Discussion

5.1 Model Performance

The classification outcomes from our FBi model provide initial, although modest, support for our central hypothesis. The linear SVM demonstrated an ability to distinguish between biperiden and placebo groups at a level significantly above chance (65.22% accuracy, $p = 0.048$). This suggests that the DCM-derived parameters do indeed capture some neurophysiological properties related to M1 receptor antagonism.

Interestingly, the RF classifier did not achieve significant predictive accuracy (58.70%, $p = 0.162$) with the same features. This could imply several things: the underlying group differences captured by these specific DCM parameters might be better suited to a linear separation, or the RF, even with hyperparameter optimization, might have been less robust to the high-dimensional nature of the feature space relative to our sample size.

The superior performance of an alternative DCM configuration (Appendix A) emphasizes that the choice of the generative model itself is an important factor influencing the information that can be extracted for classification.

5.2 Model Interpretation and Feature Importance

We looked at the most important features used by the classifiers to prove if it was indeed possible to interpret the underlying differences caused by biperiden. From previous research, we expect to see a net inhibitory effect on the intra-source activity, particularly in the pyramidal cell populations as those contain the most M1 receptors that would be blocked by the drug.

For both RF and the SVM, the majority of features in the top 20 correspond to synaptic parameters; with 17 and 15 features respectively being related to the intra-source connectivity. Of these, the H(1,3,4) is the most heavily weighted feature for both classifiers, and also the only statistically significant parameter in the t-test. H(1,3,4) corresponds to the connection strength from the inhibitory interneurons to the spiny stellate cells in the right STG. Other heavily weighted features for the RF are T(4,3) and D(1), which represent the NMDA rate constant in the rSTG and the intrinsic inter-population delay for the whole model. Looking at the posterior means of these parameters H(1,3,4) is increased in the biperiden models, while the other means are lower. The inhibitory gain being increased would indeed result in a net inhibitory effect on the canonical microcircuit as a whole, as would a lower NMDA rate constant. However, a lower intrinsic delay would imply more conductive membranes, which is against our expectation from the literature review.

We can see similar effects when looking at the three most weighted SVM parameters. H(4,3,5) corresponds to the inhibitory interneuron gain on the inferior pyramidal cells in the rIFG region, and A(5,4) corresponds to the forward connectivity between the rSTG and rIFG; the inhibitory gain is strengthened in biperiden while the connectivity is weakened. The H parameter being strengthened does cause a net inhibitory effect, as would the connectivity being weakened, however we didn't expect large changes in inter-source connectivity.

A one-by-one analysis of the parameters would not be appropriate for this report, however we observe that the other heavily weighted parameters also mostly follow this trend of causing a net inhibitory effect. This is already a notable result, since the ability to infer the net effect of a receptor antagonist by looking at how parameters change can help to identify underlying mechanisms in pathological cases. However, the fact that pyramidal cells are only being directly represented in one of the top three most important parameters for either classifier, and the potential to add a specific potassium conductivity parameter shows that there is room for refinement when it comes to modeling precise pathophysiological mechanisms. This could be achieved with an improved model, as discussed in the following section.

6 Future work

6.1 DCM

The observation of higher accuracy (73.91% for the SVM) with an alternative DCM configuration (see Appendix A), which inadvertently deviated from our primary model based on [Garrido et al. 2009], gives us an interesting direction for future work. While our main analysis is based on the theoretically-grounded model, this finding suggests that other DCM architectures might actually be better suited for modeling our MMN paradigm. Therefore, an exploration of a DCM model space and comparing the negative free energies, a proxy for the model evidence, could suggest better models. The generative embedding could then either be the posterior estimates of the winning model or a Bayesian model

average (BMA) of the whole model family. Possible model spaces could be the exploration of different forward, backward, lateral, or modulation connections as in [Garrido et al. 2008]. A different model space could consist of different prior mean and variances for specific, relevant model parameters, where one would expect a difference between the placebo and biperiden group, e.g. NMDA synaptic time constants or synaptic densities. Moreover, the dataset of the Study 2 placebo participants of [Weber et al. 2022] could be used to infer mean posterior estimates for this specific MMN paradigm. A Bayesian model average of these estimates could then be used as a prior for our actual dataset. However, the biperiden group might suffer from this optimization. Therefore, the next suggestion could be useful.

We could try to avoid potential local extrema during model inversion by using a multi-start variational Bayes as in [Schöbi et al. 2021], who found that their best models in terms of negative free energy always started from a point that was not the prior mean, which points to a potential multimodal distribution of the real parameters. [Schöbi et al. 2021] also used a custom written Runge-Kutta integration scheme (RK) as suggested by [Lemaréchal et al. 2018] which could result in more accurate posterior estimates if used in our approach. The current SPM integration scheme relies on a first-order Taylor approximation, which is computationally cheap but relies on the assumption that delays are small enough not to quickly build up errors. However, RK is computationally more heavy and requires a substantially longer computation time [Lemaréchal et al. 2018].

Another significant improvement of our current approach could be the adaptation of our neuronal model. The strongest direct impact of biperiden should be in the potassium ion current [Bolden et al. 1992; Galvin et al. 2020; Thiele 2013]. The current neuronal model considers potassium to be part of the fixed leak current. Improving the model to be able to modulate this parameter as in [Gilbert et al. 2016] leads to a more plausible biological model that could express the underlying neuronal activities in a more meaningful way. This would suggest an overall better model fit.

Moreover, the dataset we used contains a third group of participants that were given amisulpride, which is a dopamine D2/D3 receptor antagonist. This group was left out of our study completely, since [Weber et al. 2022] found no significant change of the MMN. It would be an interesting experiment, to see how our classification pipeline performs on discriminating participants given amisulpride from placebo, despite the absence of changes in MMN.

6.2 ML Classification

Further methodological refinements in the ML classifier could also enhance performance. Our ML classifiers exhibited a tendency towards predicting the placebo group, possibly caused by a slight dataset imbalance (25 placebo versus 21 biperiden); various methods exist to counteract such imbalances. Additionally, exploring other classifiers, such as an elastic net which inherently performs feature selection, or linear discriminant analysis, could be beneficial. An additional problem could lie in varying classifier performance due to the stochastic nature of the Bayesian hyperparameter optimization within the nested CV. A continuation of this study should therefore consider multiple runs on different random seeds or use a more stable procedure for hyperparameter optimization.

We would have very much liked to investigate the above suggestions, but simply didn't have time to implement them before the deadline of this project. Yet we think it is very likely that these refinements to our modeling and classification algorithm can further improve predictive accuracy and interpretability.

7 Conclusion

Despite the many options for further improvement, our results already allow us to address our primary hypothesis. The statistically significant classification accuracy achieved by our main analysis model (65.22% for the SVM), and the higher accuracy from an alternative model configuration (73.91% for the SVM, see Appendix A), demonstrate that information within EEG data from auditory MMN tasks is very likely predictive of the functional status of M1 muscarinic receptors under pharmacological manipulation.

With accuracies of 65.22% for the primary model and 73.91% for the alternative one, the predictive power, while establishing a proof-of-concept, remains modest. It remains an open question whether the current upper bound of this predictive power lies in (1) a limit of relevant information in the data, (2) imperfections in our modeling and ML classification approach to extract this information, or (3) limitations due to the relatively small sample size of 46 subjects. While imperfections in the modeling and classification pipeline (2) are likely and can be addressed by further advancements, the ultimate performance ceiling will also be influenced by the other two factors. Addressing inherent information limits in the data (1) would necessitate different data acquisition strategies or paradigms to obtain more discriminative neural signals. Similarly, overcoming sample size constraints (3), just like (1) require conducting larger-scale studies, which are huge undertakings.

Acknowledgments

Finally, we would like to thank Florian, for the valuable inputs and feedback, as well as the entire teaching team for their efforts put in the Translational Neuromodeling course. While challenging, the course was very rewarding and we had a great learning experience.

References

C Bolden, B Cusack, and E Richelson. 1992. Antagonism by antimuscarinic and neuroleptic compounds at the five cloned human muscarinic cholinergic receptors expressed in Chinese hamster ovary cells. *The Journal of Pharmacology and Experimental Therapeutics* (1992).

Olivier David, Lee Harrison, and Karl J. Friston. 2005. Modelling event-related responses in the brain. *NeuroImage* 25, 3 (2005), 756–770. https://doi.org/10.1016/j.neuroimage.2004.12.030

Karl Friston, Jérémie Mattout, Nelson Trujillo-Barreto, John Ashburner, and Will Penny. 2007. Variational free energy and the Laplace approximation. *Neuroimage* 34, 1 (2007), 220–234.

Veronica C. Galvin, Sheng Tao Yang, Constantinos D. Paspalas, Yang Yang, Lu E. Jin, Dibyadeep Datta, Yury M. Morozov, Taber C. Lightbourne, Adam S. Lowet, Pasko Rakic, Amy F.T. Arnsten, and Min Wang. 2020. Muscarinic M1 Receptors Modulate Working Memory Performance and Activity via KCNQ Potassium Channels in the Primate Prefrontal Cortex. *Neuron* 106, 4 (2020), 649–661.e4. https://doi.org/10.1016/j.neuron.2020.02.030

Marta I Garrido, Karl J Friston, Stefan J Kiebel, Klaas E Stephan, Torsten Baldeweg, and James M Kilner. 2008. The functional anatomy of the MMN: a DCM study of the roving paradigm. *Neuroimage* 42, 2 (2008), 936–944.

Marta I Garrido, James M Kilner, Klaas E Stephan, and Karl J Friston. 2009. The mismatch negativity: a review of underlying mechanisms. *Clinical neurophysiology* 120, 3 (2009), 453–463.

Jessica R. Gilbert, Mkael Symmonds, Michael G. Hanna, Raymond J. Dolan, Karl J. Friston, and Rosalyn J. Moran. 2016. Profiling neuronal ion channelopathies with non-invasive brain imaging and dynamic causal models: Case studies of single gene mutations. *NeuroImage* 124 (2016), 43–53.

Jakob Heinzle and Klaas E Stephan. 2018. Dynamic causal modeling and its application to psychiatric disorders. In *Computational Psychiatry*. Elsevier, 117–144.

E.P. Lebois, C. Thorn, J.R. Edgerton, M. Popiolek, and S. Xi. 2018. Muscarinic receptor subtype distribution in the central nervous system and relevance to aging and Alzheimer's disease. *Neuropharmacology* 136 (2018), 362–373. https://doi.org/10.1016/j.neuropharm.2017.11.018 Neuropharmacology on Muscarinic Receptors.

Jean-Didier Lemaréchal, Nathalie George, and Olivier David. 2018. Comparison of two integration methods for dynamic causal modeling of electrophysiological data. *NeuroImage* 173 (2018), 623–631. https://doi.org/10.1016/j.neuroimage.2018.02.031

Risto Näätänen, Tetsuya Shiga, Satoko Asano, and Hirooki Yabe. 2015. Mismatch negativity (MMN) deficiency: a break-through biomarker in predicting psychosis onset. *International Journal of Psychophysiology* 95, 3 (2015), 338–344.

Inês Pereira, Stefan Frässle, Jakob Heinzle, Dario Schöbi, Cao Tri Do, Moritz Gruber, and Klaas E Stephan. 2021. Conductance-based dynamic causal modeling: A mathematical review of its application to cross-power spectral densities. *NeuroImage* 245 (2021), 118662.

Dario Schöbi, Fabienne Homberg, Stefan Frässle, Heike Endepols, Rosalyn J. Moran, Karl J. Friston, Marc Tittgemeyer, Jakob Heinzle, and Klaas Enno Stephan. 2021. Model-based prediction of muscarinic receptor function from auditory mismatch negativity responses. *NeuroImage* 237 (2021), 118096.

Klaas E. Stephan, Karl J. Friston, and Chris D. Frith. 2009. Dysconnection in Schizophrenia: From Abnormal Synaptic Plasticity to Failures of Self-monitoring. *Schizophrenia Bulletin* 35, 3 (01 2009), 509–527. https://doi.org/10.1093/schbul/sbn176

Alexander Thiele. 2013. Muscarinic Signaling in the Brain. *Annual Review of Neuroscience* 36, Volume 36, 2013 (2013), 271–294.

Gaël Varoquaux, Pradeep Reddy Raamana, Denis A Engemann, Andrés Hoyos-Idrobo, Yannick Schwartz, and Bertrand Thirion. 2017. Assessing and tuning brain decoders: cross-validation, caveats, and guidelines. *NeuroImage* 145 (2017), 166–179.

Laura A. Volpicelli and Allan I. Levey. 2004. Muscarinic acetylcholine receptor subtypes in cerebral cortex and hippocampus. In *Acetylcholine in the Cerebral Cortex*. Progress in Brain Research, Vol. 145. Elsevier, 59–66. https://doi.org/10.1016/S0079-6123(03)45003-6

Lilian Aline Weber, Sara Tomiello, Dario Schöbi, Katharina V Wellstein, Daniel Mueller, Sandra Iglesias, and Klaas Enno Stephan. 2022. Auditory mismatch responses are differentially sensitive to changes in muscarinic acetylcholine versus dopamine receptor function. *Elife* 11 (2022), e74835.

Wellcome Centre for Human Neuroimaging. 2025. Statistical Parametric Mapping (SPM). https://www.fil.ion.ucl.ac.uk/spm/. Accessed: 30 May 2025.

Appendices

A Results of lateral FBi

This section presents supplementary classification results obtained using the lateral FBi variant that included bilateral connections between the two STG sources as shown in Figure 1.

A.1 RF Classifier with Lateral Connections

For the DCM with lateral connections, the Random Forest (RF) classifier achieved an accuracy of 69.57% ($p = 0.022$, chance level: 50%). The sensitivity (recall for the biperiden group) was 57.14%, and the specificity (recall for the placebo group) was 80.00%. The precision for the biperiden group was 70.59%, and the F1 score was 63.16%. The confusion matrix for this RF classifier is shown in Figure 9.

		Predicted: Biperiden	Predicted: Placebo	Total
Actual	Biperiden	12	9	21
	Placebo	5	20	25
Total		17	29	46

Figure 9: Confusion matrix for the RF classifier using DCM with lateral connections, based on nested cross-validation.

A.2 SVM Classifier with Lateral Connections

For the DCM with lateral connections, the SVM classifier achieved an accuracy of 73.91% ($p = 0.005$, chance level: 50%). The sensitivity (recall for the biperiden group) was 66.67%, and the specificity (recall for the placebo group) was 80.00%. The precision for the biperiden group was 73.68%, and the F1 score was 70.00%. The confusion matrix for this SVM classifier is shown in Figure 10.

A.3 Model Evidence

The negative free energy is a lower-bound approximation of the log model evidence [Friston et al. 2007]. A higher value is preferred. Figure 11 shows the negative free energy of both models for every subject. Summing up individual negative free energies for each model results in:

		Predicted: Biperiden	Predicted: Placebo	Total
Actual	Biperiden	14	7	21
	Placebo	5	20	25
Total		19	27	46

Figure 10: Confusion matrix for the SVM classifier using DCM with lateral connections, based on nested cross-validation.

- normal FBi: -88629
- lateral FBi: -87622

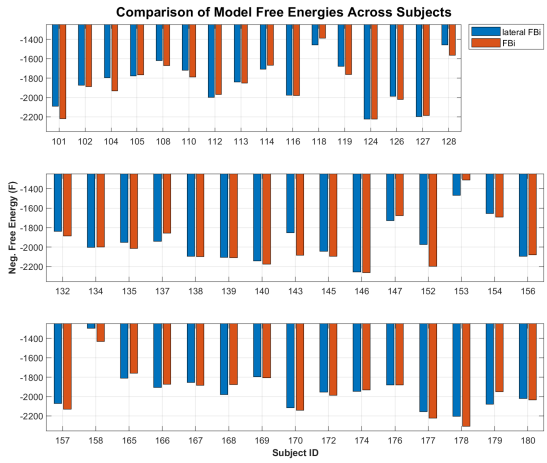

Figure 11: Subject-specific comparison of the negative free energy of the lateral FBi (blue) and normal FBi (orange).

B T-test Table

The Table 2 shows the results of the independent two-sample Bonferroni corrected t-test of the parameters of the normal FBi DCM.

Table 2: Independent Two-Sample T-Test Results (biperiden vs. placebo) for Generative Embedding Parameters of fitted FBi DCM (Bonferroni corrected alpha: $4.63 \cdot 10^{-4}$, Original alpha: 0.05, Tests: 108). An explanation of the parameters are given in Section 3.3.1.

Parameter	t-statistic	p-value (raw)	Mean Placebo	Mean Biperiden	Significance
A{1}(3, 1)	-0.5643	0.5754	-0.0018	0.0025	(Not significant)
A{1}(4, 2)	-0.2791	0.7815	-0.0197	-0.0172	(Not significant)
A{1}(5, 4)	1.4491	0.1545	0.0108	0.0034	(Not significant)
A{2}(1, 3)	-1.9140	0.0630	-0.0003	0.0002	(Not significant)
A{2}(2, 4)	1.2699	0.2108	0.0002	-0.0002	(Not significant)
A{2}(4, 5)	-1.5873	0.1198	-0.0003	0.0002	(Not significant)
AN{1}(3, 1)	-2.3878	0.0214	-0.0037	0.0008	(Not significant)
AN{1}(4, 2)	1.6797	0.1013	0.0085	0.0008	(Not significant)
AN{1}(5, 4)	-0.8215	0.4160	0.0019	0.0054	(Not significant)
AN{2}(1, 3)	-1.0406	0.3040	-0.0001	-0.0000	(Not significant)
AN{2}(2, 4)	1.8790	0.0669	-0.0000	-0.0002	(Not significant)
AN{2}(4, 5)	1.9694	0.0561	0.0008	-0.0000	(Not significant)
B{1}(1, 1)	-1.9868	0.0536	-0.0036	0.0338	(Not significant)
B{1}(3, 1)	-0.4989	0.6204	-0.0027	0.0029	(Not significant)
B{1}(2, 2)	-1.7228	0.0927	-0.0098	0.0308	(Not significant)
B{1}(4, 2)	0.5545	0.5828	0.0139	0.0053	(Not significant)
B{1}(1, 3)	-1.5950	0.1179	-0.0007	0.0001	(Not significant)
B{1}(2, 4)	1.5898	0.1193	0.0003	-0.0004	(Not significant)
B{1}(5, 4)	-0.1854	0.8537	-0.0015	0.0001	(Not significant)
B{1}(4, 5)	-0.5300	0.5988	-0.0003	0.0000	(Not significant)
BN{1}(3, 1)	-3.0203	0.0047	-0.0085	0.0012	(Not significant)
BN{1}(4, 2)	1.5742	0.1229	0.0117	0.0014	(Not significant)
BN{1}(1, 3)	-0.3399	0.7356	-0.0002	-0.0002	(Not significant)
BN{1}(2, 4)	1.4032	0.1693	0.0001	-0.0001	(Not significant)
BN{1}(5, 4)	-0.5979	0.5530	0.0013	0.0043	(Not significant)
BN{1}(4, 5)	1.9300	0.0602	0.0011	0.0000	(Not significant)
C(1)	-0.5271	0.6015	-0.0202	-0.0118	(Not significant)
C(2)	-1.2222	0.2288	-0.0106	0.0098	(Not significant)
S(1)	0.7260	0.4718	0.0300	0.0206	(Not significant)
T(1,1)	-0.0142	0.9888	0.0120	0.0121	(Not significant)
T(2,1)	-0.5920	0.5570	-0.0012	0.0051	(Not significant)
T(3,1)	-1.9739	0.0548	-0.0074	0.0102	(Not significant)
T(4,1)	1.6107	0.1146	0.0211	0.0012	(Not significant)
T(5,1)	0.4940	0.6239	0.0078	0.0013	(Not significant)
T(1,2)	1.0615	0.2945	0.0219	0.0018	(Not significant)
T(2,2)	-0.9143	0.3656	-0.0299	-0.0125	(Not significant)
T(3,2)	2.6365	0.0120	0.0105	-0.0284	(Not significant)
T(4,2)	-2.0329	0.0495	-0.0210	0.0122	(Not significant)
T(5,2)	0.2331	0.8168	-0.0063	-0.0115	(Not significant)
T(1,3)	0.2200	0.8271	-0.0223	-0.0275	(Not significant)
T(2,3)	1.8536	0.0705	-0.0408	-0.0991	(Not significant)
T(3,3)	-2.6911	0.0100	-0.0748	-0.0062	(Not significant)
T(4,3)	2.2165	0.0322	0.1044	-0.0181	(Not significant)
T(5,3)	-0.5596	0.5786	-0.0111	0.0201	(Not significant)

Continued on next page

Parameter	t-statistic	p-value (raw)	Mean Placebo	Mean Biperiden	Significance
CV(1)	0.3114	0.7571	0.0606	0.0534	(Not significant)
CV(2)	-0.0636	0.9496	0.0765	0.0776	(Not significant)
CV(3)	0.6510	0.5184	0.0161	0.0080	(Not significant)
CV(4)	-0.1498	0.8817	0.0006	0.0007	(Not significant)
E(1)	0.1221	0.9034	0.1182	0.1156	(Not significant)
H(1,1,1)	2.8274	0.0071	0.0270	-0.0112	(Not significant)
H(1,3,1)	1.0132	0.3170	0.0073	0.0018	(Not significant)
H(2,1,1)	-0.6875	0.4954	-0.0244	-0.0144	(Not significant)
H(2,2,1)	1.0587	0.2965	0.0127	-0.0031	(Not significant)
H(2,3,1)	-0.5512	0.5843	-0.0045	-0.0016	(Not significant)
H(3,1,1)	-1.3314	0.1904	-0.0047	0.0070	(Not significant)
H(3,3,1)	-0.0674	0.9466	0.0031	0.0037	(Not significant)
H(3,4,1)	0.0232	0.9816	-0.0005	-0.0005	(Not significant)
H(4,2,1)	-0.1413	0.8883	-0.0012	-0.0009	(Not significant)
H(4,3,1)	0.1613	0.8728	-0.0000	-0.0001	(Not significant)
H(4,4,1)	-0.3830	0.7036	0.0011	0.0021	(Not significant)
H(1,1,2)	0.2645	0.7926	-0.0092	-0.0130	(Not significant)
H(1,3,2)	0.4165	0.6798	-0.0037	-0.0062	(Not significant)
H(2,1,2)	0.6597	0.5133	-0.0187	-0.0310	(Not significant)
H(2,2,2)	-0.5518	0.5840	-0.0133	-0.0040	(Not significant)
H(2,3,2)	0.9423	0.3512	-0.0014	-0.0053	(Not significant)
H(3,1,2)	1.7898	0.0807	-0.0013	-0.0160	(Not significant)
H(3,3,2)	-0.7340	0.4677	0.0118	0.0198	(Not significant)
H(3,4,2)	0.4810	0.6329	0.0009	-0.0001	(Not significant)
H(4,2,2)	-0.2252	0.8230	0.0007	0.0012	(Not significant)
H(4,3,2)	0.0867	0.9315	0.0003	0.0002	(Not significant)
H(4,4,2)	0.9266	0.3595	-0.0000	-0.0021	(Not significant)
H(1,1,3)	1.8572	0.0700	-0.0103	-0.0288	(Not significant)
H(1,3,3)	1.8920	0.0658	0.0004	-0.0097	(Not significant)
H(2,1,3)	0.1930	0.8478	0.0284	0.0265	(Not significant)
H(2,2,3)	-1.0414	0.3035	-0.0511	-0.0382	(Not significant)
H(2,3,3)	0.9198	0.3640	-0.0005	-0.0028	(Not significant)
H(3,1,3)	-1.2632	0.2134	-0.0111	-0.0055	(Not significant)
H(3,3,3)	1.0071	0.3194	0.0123	0.0027	(Not significant)
H(3,4,3)	-0.9370	0.3542	-0.0019	-0.0009	(Not significant)
H(4,2,3)	0.9385	0.3531	0.0015	0.0001	(Not significant)
H(4,3,3)	-0.2614	0.7951	-0.0000	0.0001	(Not significant)
H(4,4,3)	-0.9191	0.3642	-0.0003	0.0016	(Not significant)
H(1,1,4)	-2.7002	0.0102	-0.0530	0.0018	(Not significant)
H(1,3,4)	-3.8917	0.0004	-0.0190	0.0144	Significant ($p < 4.63 \cdot 10^{-4}$)
H(2,1,4)	1.3454	0.1869	0.0408	0.0190	(Not significant)
H(2,2,4)	1.1180	0.2711	-0.0470	-0.0643	(Not significant)
H(2,3,4)	-1.6016	0.1174	-0.0105	-0.0011	(Not significant)
H(3,1,4)	-0.4672	0.6427	-0.0067	-0.0022	(Not significant)
H(3,3,4)	0.4705	0.6403	-0.0067	-0.0127	(Not significant)
H(3,4,4)	0.5995	0.5522	-0.0021	-0.0040	(Not significant)
H(4,2,4)	-1.2482	0.2190	-0.0091	-0.0031	(Not significant)
H(4,3,4)	1.9667	0.0556	0.0009	-0.0004	(Not significant)
H(4,4,4)	0.7594	0.4517	0.0121	0.0060	(Not significant)
H(1,1,5)	0.8756	0.3866	-0.0385	-0.0523	(Not significant)

Continued on next page

Parameter	t-statistic	p-value (raw)	Mean Placebo	Mean Biperiden	Significance
H(1,3,5)	1.5573	0.1281	-0.0199	-0.0334	(Not significant)
H(2,1,5)	-0.7398	0.4644	0.0271	0.0358	(Not significant)
H(2,2,5)	-1.7059	0.0962	-0.0428	-0.0118	(Not significant)
H(2,3,5)	0.9347	0.3559	-0.0020	-0.0065	(Not significant)
H(3,1,5)	-0.0466	0.9630	-0.0094	-0.0090	(Not significant)
H(3,3,5)	-0.3384	0.7367	0.0119	0.0165	(Not significant)
H(3,4,5)	-0.6287	0.5329	-0.0013	0.0006	(Not significant)
H(4,2,5)	1.4033	0.1679	0.0061	-0.0004	(Not significant)
H(4,3,5)	-2.2165	0.0320	-0.0013	0.0003	(Not significant)
H(4,4,5)	-0.6750	0.5033	-0.0095	-0.0036	(Not significant)
R(1)	2.1010	0.0420	-0.0135	-0.0892	(Not significant)
R(2)	-2.2378	0.0304	-0.0566	0.0768	(Not significant)
D(1)	1.6371	0.1109	-0.0005	-0.0116	(Not significant)
D(2)	-1.0256	0.3117	-0.0213	-0.0126	(Not significant)